Coordination Complexes of 1-(4-[*N-tert*-Butyl-*N*-aminoxyl]phenyl)-*1H*-1,2,4-triazole with Paramagnetic Transition Metal Dications

Lora M. Field and Paul M. Lahti*

Department of Chemistry, University of Massachusetts, Amherst, Massachusetts 01003

Received July 30, 2003

1-(4-(*N-tert*-Butyl-*N*-aminoxylphenyl))-*1H*-1,2,4-triazole (NIT-Ph-Triaz) forms isostructural cyclic 2:2 dimeric complexes with M(hfac)$_2$, M = Mn, Ni, Co, hfac = hexafluoroacetylacetonate. For M = Cu, only a sufficient sample for crystallographic analysis was isolated. For M = Mn, Ni, and Co, the M–NIT exchange is strongly antiferromagnetic. The intradimer exchange coupling between M–NIT units is $J/k = +0.53$ K for M = Mn, $J/k = (–)3.5$ K for M = Ni. For M = Co, $J/k < 0$ K, with the magnetic susceptibility tending toward zero at low temperatures. The exchange behavior is consistent with an intradimer spin polarization mechanism linking M–NIT units through the conjugated π-system of the radical. Computational modeling of NIT-Ph-Triaz gives Mulliken spin populations in good accord with experimental electron spin resonance hyperfine coupling constants, and is consistent with the presumed radical spin density distribution in the complexes. The results provide useful guidelines to anticipate spin polarization effects in organic π-radical building blocks in magnetic materials, particularly when qualitative connectivity-based analyses are clouded by nonalternant molecular connectivities.

Introduction

Various studies have probed the exchange interactions and magnetic properties of coordination complexes between stable organic radicals and paramagnetic cations as functions of structure and crystal packing. While there is a significant body of work[1] describing such complexes with both non-conjugated and conjugated organic radicals, a wealth of choices remains to be investigated.

We have previously reported[2] the structure and properties of 2:2 cyclic complexes of conjugated organic radical 5-(4-[*N-tert*-butyl-*N*-aminoxyl]phenyl)pyrimidine, **1**, with manganese(II) hexafluoroacetylacetonate and copper(II) hexaflu-

oroacetylacetonate (M(hfac)$_2$). By altering the spin distribution in the coordinating radical while maintaining structural similarity in the complex, we aimed to alter the structure and properties in an incremental manner that would allow clear magnetostructural analysis. In this Article, we report details of the synthesis and structural characterization of cyclic 2:2 coordination complexes of 1-(4-(*N-tert*-butyl-*N*-aminoxylphenyl))-*1H*-1,2,4-triazole, **2**, with Cu(II), Mn(II), Ni(II), and Co(II) hexafluoroacetylacetonates, as well as magnetic properties of the latter three systems.

1   **2**
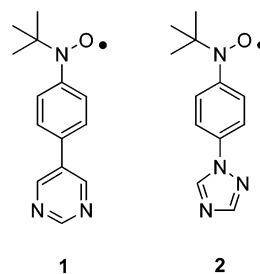
Results

Synthesis. Figure 1 shows the synthesis of nitroxide **2** and its complexation to make **3**−**6**. The silyl ether protected hydroxylamine boronic acid **7** was coupled with com-

* To whom correspondence should be addressed. E-mail: Lahti@chem.umass.edu.
 (1) (a) Caneschi, A.; Gatteschi, D.; Sessoli, R.; Rey, P. *Acc. Chem. Res.* **1989**, *22*, 392. (b) Caneschi, A.; Gatteschi, D.; Sessoli, R. In *Magnetic Molecular Materials*; Gatteschi, D., Kahn, O., Miller, J. S., Palacio, F., Eds.; Kluwer: Dordrecht, The Netherlands, 1991; p 215. (c) Gatteschi, D.; Rey, P. In *Magnetic Properties of Organic Materials*; Lahti, P. M., Ed.; Marcel Dekker: New York, 1999. (d) Iwamura, H.; Inoue, K.; Hayamizu, T. *Pure Appl. Chem.* **1996**, *68*, 243. (e) Miller, J. S.; Epstein, A. J. *MRS Bull.* **2000**, *25*, 21−30. (f) *Molecular Magnetism: New Magnetic Materials*; Itoh, K., Kinoshita, M., Eds.; Gordon and Breach: Newark, NJ, 2000. (g) Kahn, O. *Molecular Magnetism*; VCH: New York, 1993.
 (2) (a) Field, L. M.; Lahti, P. M.; Palacio, F. *Chem. Commun.* **2002**, 636. (b) Field, L. M.; Lahti, P. M.; Palacio, F.; Paduan-Filho, A. *J. Am. Chem. Soc.* **2003**, *125*, 10110.
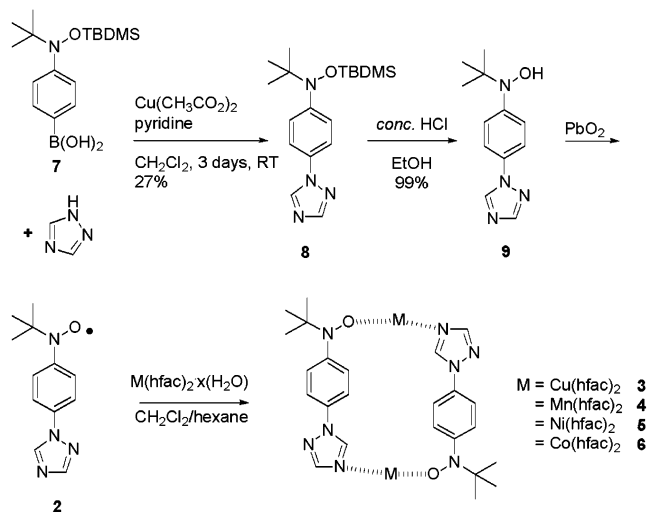
Figure 1. Synthesis of radical **2** and complexes **3**−**6**.

Although complex **3** in multiple efforts formed only in very small amounts insufficient for magnetic analysis, complexes **4**−**6** formed readily. All were stable to ambient conditions for months at least. Figure 2 shows ORTEP diagrams for each structure, while Table 1 gives summary crystallographic and structural information for each. We did not isolate any related complexes, despite varying the ratios of **2** to M(hfac)$_2$ and other crystallization conditions.

Magnetic susceptibility χ was measured for **4**−**6** over 1.8−300 K at 1000 Oe. The susceptibilities were corrected for temperature independent contributions by extrapolating their high temperature χT versus T behavior. Similar results were obtained by corrections based on diamagnetic contributions from the sample containers and Pascal's constant estimates for the complexes. Figures 3−5 show corrected χT versus T plots for **4**−**6**. The magnetization of each compound was also measured at 1.8 K as a function of applied field from 0 to 5 kOe. These plots are shown in the figures as insets.

Discussion

Crystallography. Complexes **4**−**6** are essentially isostructural, save for variation of the paramagnetic dication centers. All have triclinic $P\bar{1}$ lattices, with similar lattice dimensions. There are no unusual close contacts between molecules, so their magnetic behavior should be dominated by intramolecular, intradimer exchange. The environment about the metal centers is pseudo-octahedral in all. Copper complex **3** exhibits axial elongation of the Cu−O(1)N(1) bond and the Cu−O(5) hfac bond *trans* to it (Table 2), but

mercially available 1*H*-1,2,4-triazole to give **8**, deprotected to hydroxylamine **9**, and oxidized to **2**. Although **9** was stable and readily characterized by spectral, elemental, and crystallographic methods, radical **2** was somewhat unstable in solution. We obtained spectral and crystallographic analysis for **2**, but we had to make and use it fairly quickly to minimize solution decomposition. Interestingly, the instability of **2** did not seem to hinder our ability to make complexes **4**−**6** by slow precipitation from layered solutions of **2** with the appropriate M(hfac)$_2$ compound in air. Perhaps the initial stages of complexation between **2** and the M(II) cations stabilize the radical somewhat to decomposition.
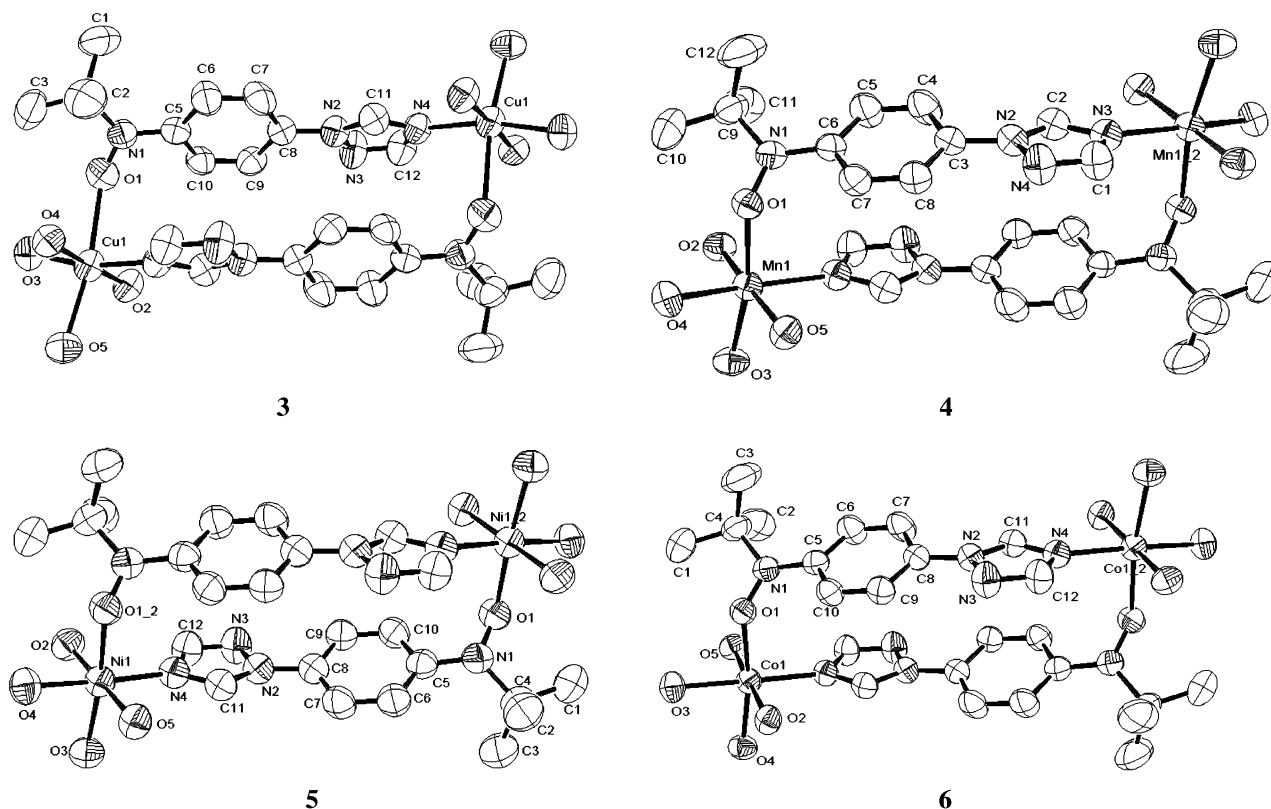

Figure 2. ORTEP diagrams of complexes **3**−**6**. Hydrogens and uncoordinated atoms of the hfac groups are omitted for clarity of viewing.

Table 1. Crystallographic Analysis Parameters for **3**−**6**

|	**3**	**4**	**5**	**6**
chemical formula	$C_{22}H_{17}F_{12}CuN_4O_5$	$C_{22}H_{17}F_{12}MnN_4O_5$	$C_{22}H_{17}F_{12}NiN_4O_5$	$C_{22}H_{17}F_{12}CoN_4O_5$
fw	708.917	700.32	704.087	704.31
cell setting, space group	triclinic, $P\bar{1}$	triclinic, $P\bar{1}$	triclinic, $P\bar{1}$	triclinic, $P\bar{1}$
a, b, c (Å)	10.1436(3)	9.7110(2)	9.8155(2)	9.73670(10)
	10.3358(3)	10.6770(3)	10.5185(2)	10.5646(2)
	14.9004(6)	14.7440(6)	15.0198(3)	14.8865(3)
α, β, γ (deg)	91.7513(11)	93.1760(12)	93.1995(7)	93.0482(6)
	93.5277(13)	91.2500(12)	92.5002(8)	91.6094(6)
	114.6025(10)	114.458(2)	116.6025(8)	115.4709(10)
V (Å^3)	1414.96(8)	1387.70(7)	1380.29(5)	1378.29(4)
Z	2	2	2	2
D_x (Mg/m^3)	1.664	1.676	1.694	1.697
radiation type	Mo Kα	Mo Kα	Mo Kα	Mo Kα
θ range (deg)	4.12−25.02	4.16−25.10	4.09−25.07	4.12−25.04
$F(000)$	708	700	706	704
μ (mm^{-1})	0.891	0.597	0.825	0.745
cryst color	green needle	red needle	green needle	green needle
data collection method	$\omega-2\theta$ scans	$\omega-2\theta$ scans	$\omega-2\theta$ scans	$\omega-2\theta$ scans
collected/unique reflns	8881/4935	8274/4874	8751/4819	9015/4833
criterion for obsd reflns	$I > 2\sigma(I)$	$I > 2\sigma(I)$	$I > 2\sigma(I)$	$I > 2\sigma(I)$
R_{int}	0.0336	0.0299	0.0207	0.0176
range of h,k,l	$-12 \rightarrow h \rightarrow 11$	$-9 \rightarrow h \rightarrow 11$	$-11 \rightarrow h \rightarrow 11$	$-11 \rightarrow h \rightarrow 11$
	$-12 \rightarrow k \rightarrow 12$	$-13 \rightarrow k \rightarrow 12$	$-12 \rightarrow k \rightarrow 12$	$-12 \rightarrow k \rightarrow 12$
	$-17 \rightarrow l \rightarrow 17$	$-17 \rightarrow l \rightarrow 17$	$-17 \rightarrow l \rightarrow 17$	$-17 \rightarrow l \rightarrow 17$
completeness to 2θ	0.99	0.98	0.98	0.99
reflns, restraints, params	4935/0/399	4874/0/399	4819/0/399	4833/0/397
H-atom treatment	Refxyz	Refxyz	Refxyz	Refxyz
GOF on F^2	1.033	1.366	1.032	1.029
$\Delta\rho_{max}, \Delta\rho_{min}$ (e·Å^{-3})	0.773, −0.563	0.973, −0.499	0.254, −0.140	0.862, −0.470
R1, wR2 ($I > 2\sigma(I)$)	0.0694, 0.1798	0.0692, 0.1900	0.0492, 0.1315	0.0526, 0.1414
R1, wR2 (all)	0.1068, 0.2060	0.0927, 0.2027	0.0545, 0.1375	0.0588, 0.1484
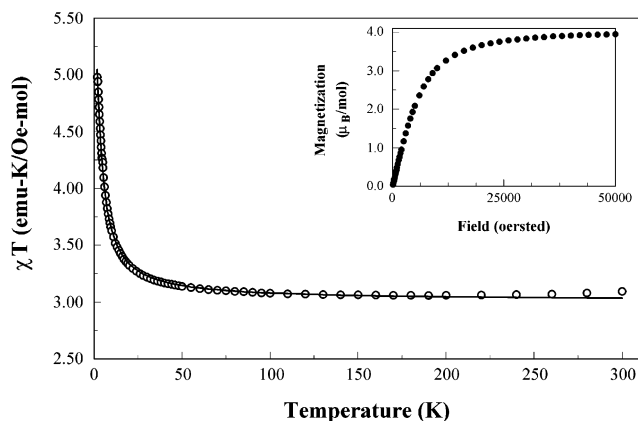
Figure 3. χT versus T plot for **4**. Solid line is the fit of the data to eq 1 in the text. Inset shows magnetization versus field at 1.8 K.

Figure 4. χT versus T (a) and χ versus T (b) plots for **5**. Solid line in curve b is the fit of the data to eq 2 in the text. Inset shows magnetization versus field at 1.8 K.

otherwise, the bond lengths and angles about the metal centers are comparable.

Magnetism. Since the molecular and crystallographic natures of **3**−**6** are so similar, their magnetic exchange mechanisms should be closely related save for variations in the cations. We presume that exchange between M−NIT sites will occur by an intramolecular spin polarization mechanism, since the closest intramolecular metal−metal distances are nearly 11 Å, while the nearest intermolecular metal−metal distances are about 7 Å. Any through bond exchange mechanism should depend on the planarity of the π-conjugated portions of the structure. The phenyl-triazole torsion is 15−19°, and the phenyl-nitroxide torsion is 19−23°. Neither range is large, so π-conjugation is not much compromised.
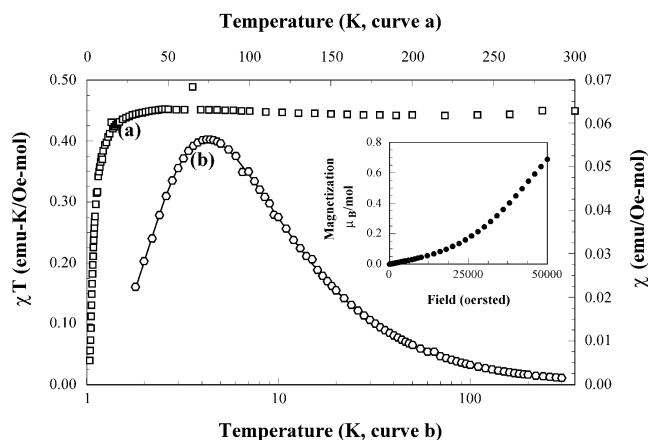
Manganese complex **4** showed a high temperature value of χT of about 3.1 (emu K)/(Oe mol), in close agreement with the value of 3.001 (emu K)/(Oe mol) expected where M−NIT has $S = 2$, with strong antiferromagnetic (AFM) coupling between Mn(II) and the coordinated nitroxide. The magnetization plot at 1.8 K saturates at 4.0 μ_B/mol for the half-dimer molecular weight, consistent with the value expected for $S = 2$ spin units.

The upturn in the χT versus T plot for **4** indicates ferromagnetic (FM) coupling between the Mn−NIT spin units and should follow eq 1.[3] In the equation, g_{av} is the average Landé constant for the component spin units, k is

(3) Derived from the van Vleck equation. For the derivation, see for example ref 1g, pp 5−7, and 112ff.

Table 2. Selected Structural Parameters for **3−6**[a]

	3	**4**	**5**	**6**
M−O bond lengths (hfac)	Cu(1)−O(2) 1.949(4)	Mn(1)−O(2) 2.137(3)	Ni(1)−O(2) 2.015(2)	Co(1)−O(5) 2.046(2)
	Cu(1)−O(4) 1.952(4)	Mn(1)−O(4) 2.154(3)	Ni(1)−O(5) 2.028(2)	Co(1)−O(2) 2.060(2)
	Cu(1)−O(3) 1.977(4)	Mn(1)−O(5) 2.169(3)	Ni(1)−O(4) 2.042(2)	Co(1)−O(4) 2.090(2)
	Cu(1)−O(5) 2.249(4)	Mn(1)−O(3) 2.175(3)	Ni(1)−O(3) 2.056(2)	Co(1)−O(3) 2.093(2)
M−ON bond length	Cu(1)−O(1) 2.548(4)	Mn(1)−O(1) 2.149(3)	Ni(1)−O(1) 2.081(2)	Co(1)−O(1) 2.091(2)
M−N bond length	Cu(1)−N(4) 1.998(4)	Mn(1)−N(3) 2.222(4)	Ni(1)−N(4) 2.054(3)	Co(1)−N(4) 2.109(3)
N−O bond length	O(1)−N(1) 1.288(6)	O(1)−N(1) 1.298(4)	O(1)−N(1) 1.294(3)	O(1)−N(1) 1.295(3)
M···M intradimer distance	Cu(1)···Cu(1)′ 10.977(1)	Mn(1)···Mn(1)′ 10.950(1)	Ni(1)···Ni(1)′ 10.809(1)	Co(1)···Co(1)′ 10.794(1)
phen−NO torsion	O(1)−N(1)−C(5)−C(10) −17.46(64)	O(1)−N(1)−C(6)−C(7) −22.58(46)	O(1)−N(1)−C(5)−C(10) −20.24(33)	O(1)−N(1)-C(5)−C(10) −20.35(34)
phen−triaz torsion	N(3)−N(2)−C(8)−C(9) −19.36(65)	N(4)−N(2)−C(3)−C(8) −14.87(50)	N(3)−N(2)−C(8)−C(9) −15.75(36)	N(3)−N(2)−C(8)−C(9) −15.80(36)

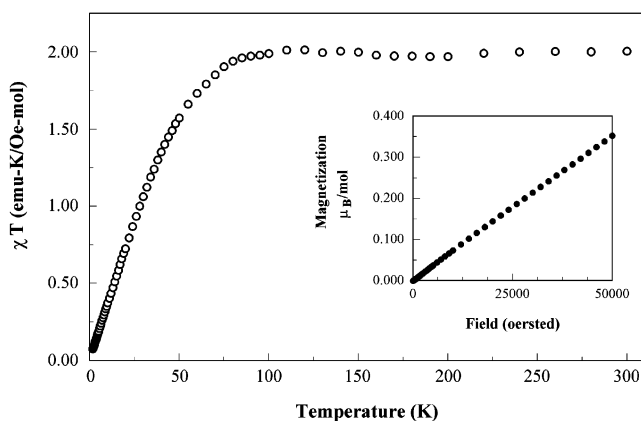[a] All bond lengths in angstroms, all angles in degrees.

Figure 5. χT versus T plot for **6**. Inset shows magnetization versus field at 1.8 K.

the Boltzmann constant, μ_B is the Bohr magneton constant, N_0 is Avogadro's number, θ is a mean field term, and J/k is the exchange constant. We found the best fit with $J/k = +0.53$ K, $\theta = +0.07$ K, using $g_{av} = 2.004$. The small mean field term confirms that the spin sites do not experience significant longer range interactions, other than pairwise M−NIT FM coupling. We will describe here an intramolecular exchange model for this behavior.

$$\chi T = \frac{T \cdot N_0 g_{av}^2 \mu_B^2}{k(T - \theta)} \cdot$$
$$\frac{84 + 6 \exp(-10J/kT) + 30 \exp(-6J/kT) + 180 \exp(8J/kT)}{7 + \exp(-12J/kT) + 3 \exp(-10J/kT) + 5 \exp(-6J/kT) + 9 \exp(8J/kT)} \quad (1)$$

Complex **5** exhibits a high temperature limiting χT value of about 0.45 (emu K)/(Oe mol), consistent with a system of $S = \frac{1}{2}$ spin units having $g > 2$. Using eq 2 where all constants have the meanings already given, the high temperature χT is consistent with $S = \frac{1}{2}$, $g_{av} = 2.19$, showing strong AFM Ni−NIT coupling.

$$\chi T = \frac{N_0 g_{av}^2 \mu_B^2}{3k} S(S + 1) \quad (2)$$

As temperature decreases, the susceptibility χ of **5** maximizes at about 4.8 K and then decreases, indicating onset of AFM exchange interactions. On the basis of the structure of **5**, we assumed that spin pairing of the Ni−NIT units was

occurring. The magnetization plot, which does not saturate at fields up to 50 kOe, supports this; the plot rises gently at first, and then more swiftly at higher fields. This shape is consistent with the early portion of a typical S-curve expected[4] for magnetization of an $S = 0$ state system that undergoes spin state crossover at higher magnetic fields, whereby a quantum level of a paramagnetic excited state is driven below the $S = 0$ ground state due to Zeeman splitting.

We fitted the χ versus T data for **5** to the Bleaney−Bowers[5] type eq 3, where the constants have the meanings described earlier.

$$\chi = \frac{N_0 g_{av}^2 \mu_B^2}{k(T - \theta)} \times \frac{\exp(-2J/kT)}{1 + 3 \exp(-2J/kT)} \quad (3)$$

Figure 4 shows a good fit to the data for $g_{av} = 2.24$, $J/k = -3.5$ K, and $\theta = +0.17$ K. As with **5**, the small mean field constant shows that there is very little interaction between spin sites other than the spin pairing exchange. The observed g-value is fairly typical for nickel complexes.[6] Since there are no close crystallographic interdimer contacts, we assign the Ni−NIT spin pairing to an intramolecular exchange pathway described in more detail in the following section.

We did not attempt detailed analysis of system **6**, due to the complexity of accounting for spin−orbit coupling effects in octahedral Co(II) and its known effective Kramers' doublet state at lower temperatures.[7] The χT versus T plot is essentially flat at 2.0 (emu K)/(Oe mol) for $T > 150$ K, while the magnetization plot is linear up to the maximum measured field of 50 kOe. The high temperature χT corresponds to a magnetization of about 4 μ_B/mol for the half-dimer molecular weight. In an octahedral environment, Co(II) at room

(4) An example of the behavior of magnetization under spin crossover conditions for an organic diradical system with near-degenerate singlet and triplet states is given in: Matsuda, K.; Iwamura, H. *J. Chem. Soc., Perkin Trans. 2* **1998**, *5*, 1023−1026. For a discussion of magnetization under spin crossover conditions for dimers related to those in this article, see ref 2b.
(5) Bleaney, B.; Bowers, K. D. *Proc. R. Soc. London, Ser. A* **1952**, 214.
(6) (a) Salerno, J. C. In *The Bioinorganic Chemistry of Nickel*; Lancaster, J. R., Jr., Ed.; VCH: New York, 1988; p 53. (b) Lippin, A. G.; McAuley, A. *Adv. Inorg. Chem.* **1988**, *32*, 241. (c) Nag, K.; Chakravorty, A. *Coord. Chem. Rev.* **1980**, *33*, 87.
(7) Carlin, R. L. *Magnetochemistry*; Springer-Verlag: Berlin, Germany 1986; pp 65−67.

temperature contributes 4.7−5.2 μ_B/mol to the sample magnetization.[5] Given the significantly lower observed value, the Co−NIT group appears to be antiferromagnetically coupled, as expected for reasons described in the following section. The χT versus T plot clearly trends to zero at low temperatures, so AFM spin pairing of Co−NIT units appears to occur in a manner qualitatively similar to **5**.

Exchange Mechanisms. It is regrettable that we could not make more than a few milligrams of **3**, since it would have been an interesting magnetic comparison to the other systems. In **4**, the AFM exchange between Mn(II) and the NIT unit in a pseudo-octahedral environment is well-precedented. This can be explained[8] in terms of nonzero overlap between magnetic d-orbitals of Mn(II) with the NIT π^*-type singly occupied molecular orbital (SOMO) for any octahedral coordination site. Ni(II) and Co(II) are strongly AFM exchange coupled to a pseudo-octahedral axial NIT unit for similar reasons.

The exchange coupling between spin sites provides the most useful insights for our goal of understanding exchange as a function of structural variation. The FM exchange between Mn−NIT units in **4** is virtually the same as behavior observed for the parity analogue **10** studied by Ishimaru et al.,[9] who found $J/k = +0.59$ K between two effectively $S = 2$Mn−(4-NIT-Ph-Im) units by the model of eq 1. The modest heteroatom perturbation of changing 1,2,4-triazole for imidazole in **4** versus **10** does not make a significant difference to the exchange. However, the behaviors of both **4** and **10** are qualitatively opposite to the AFM exchange coupling of $J/k = -0.25$ K between Mn−(4-NIT-Ph-Pyrim) units in **11** previously reported[2] by us, despite the fact that **4**, **10**, and **11** have the same number of atoms connecting Mn(II) ions together in circuits within the dimers, with heteroatom placement in the same positions of the circuits.
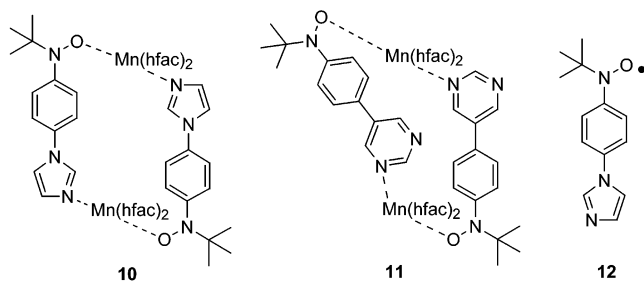
In order to explain the relative behaviors of the Mn(II)-containing systems, we considered the spin distributions in the organic radical fragments. The nonalternant, heterosubstituted rings in **4** and **10** are the keys to reversing their qualitative exchange behaviors relative to **11**. UB3LYP/6-31G* computations[10,11] at the crystallographic geometries of models for the radical portions of the complexes (Table 3) show that the spin density on the coordinated nitrogens of **4** and **10** has the same sign as the nitroxide unit; the opposite
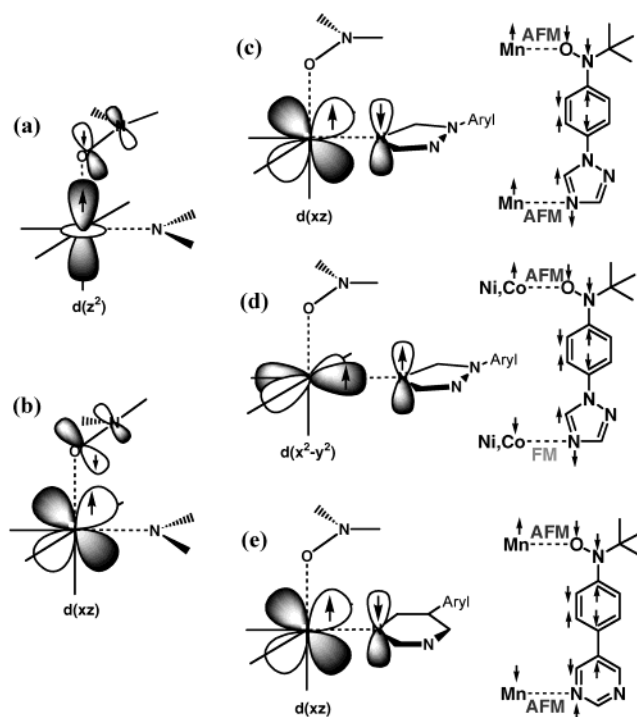

Figure 6. Qualitative orbital and parity based models for exchange mechanisms in **4**−**6** and **11**.

is the case in **11**, as shown in Figure 6. The computational results are in reasonable accord with electron spin resonance (ESR) hyperfine coupling constant data obtained for radicals **1**, **2**, and **12** in solution, as shown in Table 3. Crucially, the ESR hyperfine coupling on the coordinated 4-position of the triazolyl ring in **2** is 0.2−0.4 G (depending on the assignment of nitrogen hyperfine), while that on pyrimidine nitrogen in **1** is too small to resolve. The experimental spin population on the coordinated nitrogen in **4** is thus significantly larger than that on the analogous nitrogen in **11**, qualitatively consistent with the larger exchange strength in **4**. Although we are not aware whether a similar hyperfine coupling analysis of radical **12** has been given,[12] it would be surprising if it were substantially different from the computed results, given the similarity in behaviors of **4** and **7**. While the experiments do not reveal the sign of the spin density on the coordinated nitrogens, the relative signs of exchange in **4** and **11** strongly support the qualitative descriptions in Figure 6.

(8) Caneschi, A.; Gatteschi, D.; Sessoli, R.; Rey, P. *Acc. Chem. Res.* **1989**, *22*, 392.
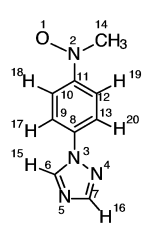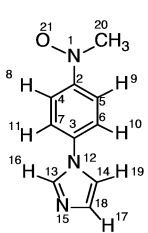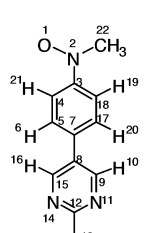
(9) Ishimura, Y.; Inoue, K.; Koga, N.; Iwamura, H. *Chem. Lett.* **1994**, 1693.

(10) Becke, A. D. *J. Chem. Phys.* **1993**, *98*, 5648.

(11) All computations were carried out using Gaussian 98: Frisch, M. J.; Trucks, G. W.; Schlegel, H. B.; Scuseria, G. E.; Robb, M. A.; Cheeseman, J. R.; Zakrzewski, V. G.; Montgomery, J. A., Jr.; Stratmann, R. E.; Burant, J. C.; Dapprich, S.; Millam, J. M.; Daniels, A. D.; Kudin, K. N.; Strain, M. C.; Farkas, O.; Tomasi, J.; Barone, V.; Cossi, M.; Cammi, R.; Mennucci, B.; Pomelli, C.; Adamo, C.; Clifford, S.; Ochterski, J.; Petersson, G. A.; Ayala, P. Y.; Cui, Q.; Morokuma, K.; Malick, D. K.; Rabuck, A. D.; Raghavachari, K.; Foresman, J. B.; Cioslowski, J.; Ortiz, J. V.; Stefanov, B. B.; Liu, G.; Liashenko, A.; Piskorz, P.; Komaromi, I.; Gomperts, R.; Martin, R. L.; Fox, D. J.; Keith, T.; Al-Laham, M. A.; Peng, C. Y.; Nanayakkara, A.; Gonzalez, C.; Challacombe, M.; Gill, P. M. W.; Johnson, B. G.; Chen, W.; Wong, M. W.; Andres, J. L.; Head-Gordon, M.; Replogle, E. S.; Pople, J. A. *Gaussian 98*; Gaussian, Inc.: Pittsburgh, PA, 1998.

(12) The nitroxide hyperfine coupling for **12** is given in: Ishimaru, Y.; Makoto Kitano, M.; Kumada, H.; Koga, N.; Iwamura, H. *Inorg. Chem.* **1998**, *37*, 2273.

Table 3. UB3LYP/6-31G* Mulliken Spin Densities and ESR Hyperfine Coupling (hfc) in Models for Radicals **2**, **12**, and **1**[a]

Radical	Atom numbers, ρ(spin), and (experimental/computed hfc)	
(structure diagram, radical 2)	1 O 0.536 2 N 0.392 (exp = 11.30 G, *theor** = 9.4 G*) 3 N -0.004 (exp = 0.43 G, *theor** =(-)0.2 G*) 4 N 0.0006 (exp < 0.1 G, *theor** = 0.04 G*) *5 N 0.002 (exp = 0.18 G, *theor** = 0.03 G*) 6 C 0.006 7 C 0.003 8 C 0.055 9 C -0.029 10 C 0.058 11 C -0.054 12 C 0.061	13 C -0.029 14 C -0.030 15 H -0.0003 (exp = 0.11 G, *theor** = (-)0.18 G* 16 H -0.0002 17 H 0.001 18 H -0.003 19 H -0.002 (exp = 2.34 G, *theor** = (-)2.0 G* 20 H 0.001 (exp = 0.93 G, *theor** = 0.8 G*
(structure diagram, radical 12)	1 N 0.341 (exp*** = 11.87 G, *theor** = 7.3 G*) 2 C -0.097 3 C 0.114 4 C 0.121 5 C 0.117 6 C -0.063 7 C -0.061 8 H -0.006 9 H -0.005 (*theor** = (-)2.7 G*) 10 H 0.002 (*theor** = 1.1 G*) 11 H 0.002 12 N -0.004	13 C 0.007 14 C 0.001 *15 N 0.003 (*theor** = 0.05 G*) 16 H -0.0003 17 H -0.0002 18 C 0.005 19 H -0.00004 20 C -0.030 21 O 0.515
(structure diagram, radical 1)	1 O 0.529 2 N 0.369 (exp = 11.70 G, *theor = 8.6 G*) 3 C -0.076 4 C 0.090 5 C -0.047 6 H 0.002 7 C 0.089 8 C -0.015 9 C 0.014 10 H -0.0005 11 N -0.005 (exp < 0.02 G, *theor = (-)0.1 G*) 12 C 0.012	13 H -0.0007 *14 N -0.006 (exp < 0.1 G, *theor = (-)0.1 G*) 15 C 0.013 16 H -0.0005 17 C -0.047 18 C 0.090 19 H -0.004 (exp = 2.11 G, *theor = (-)2.0 G*) 20 H 0.002 (exp = 0.94 G, *theor = 0.8 G*) 21 H -0.004 22 C -0.030

[a] A single asterisk indicates coordinated nitrogen. Two asterisks indicate that experimental and computed hyperfine coupling constants are given in gauss as (exp = 1.00 G, *theor = 1.00 G*). All hfc taken directly from Gaussian 98 output (see ref 11). Values marked with three asterisks were taken from ref 12.

The AFM exchange coupling between Ni(II)−NIT units in complex **5** is interesting by comparison to the FM coupling between Mn(II)−NIT units in **4**, since the two complexes are structurally almost identical. The different metal ion magnetic orbitals that overlap with the spin-polarized π-system of the triazole ring give the observed behaviors. Figure 6 shows orbital models to support the observed M−NIT exchange and proposed intradimer spin polarization pathways for **4**−**6**, with comparison to the analogous pathway for **11**. Depending on geometry, either the d_{z^2} or d_{xz} can overlap with the NIT π*-SOMO to give AFM M−NIT exchange (situations a and b in the figure). Mn(II), Ni(II), and Co(II) all have magnetic d_{z^2} orbitals, so **4**−**6** and **10**−**11** are all expected to exhibit AFM M−NIT exchange coupling as observed. No matter what the geometry of a coordinating triazole or pyrimidine ring, there must be some overlap of the organic ligand π-space with a Mn(II) magnetic orbital, favoring AFM exchange in situation c. By contrast, the Ni(II) magnetic orbitals are orthogonal to the triazole π-orbitals, so FM exchange becomes favored in situation d. We presume the exchange mechanism for Co(II) to be similar to that for Ni(II), on the basis of the observed χT versus T data for **6**. In the final comparison, the exchange pathway through the pyrimidine ring, situation e, is analogous to situation c. These magnetic orbital overlap mechanisms for

the metal cations with the NIT π*-SOMO and the aza-ligands clearly and self-consistently explain the qualitative exchange behaviors of **4**−**6** and **10**−**11**.

Conclusions

We synthesized nitroxide radical **2**, which has an unusual degree of spin delocalization through the phenyl ring onto the nonalternant triazole ring that forms the coordination pathway to the paramagnetic dications. The delocalization may be partly responsible for its instability in some types of solution. We made and crystallographically characterized cyclic, 2:2 coordination complexes of **2** with Cu(II), Mn-(II), Co(II), and Ni(II), the latter three in sufficient quantities for magnetic analysis. The complexes are isostructural and crystallographically isomorphous. All showed strong antiferromagnetic M−NIT exchange: the Mn(II) complex showed ferromagnetic exchange between M−NIT units, while the Co(II) and Ni(II) complexes showed antiferromagnetic spin pairing. These behaviors are consistent with qualitative spin parity and orbital overlap models.

By using the nonalternant ring system (triazole) as the coordinating ligand, we appear to have reversed the parity of the spin density on the coordinating site by comparison to a corresponding alternant (pyrimidine) ligand that yields the same length and atom placements in a cyclic 2:2 complex.

Such modulation of exchange behavior by minor changes in structure is an example of the highly controlled variation possible in constructing magnetic materials from molecular building blocks.

Experimental Section

General. X-ray crystallographic analyses were carried out by Dr. A. Chandrasekaran at the X-ray Structural Characterization Facility at UMass-Amherst. Elemental analysis was carried out by Dr. G. Dabkowski of the UMass-Amherst Microanalysis Laboratory. Melting points are uncorrected. All magnetic measurements were obtained at the UMass-Amherst Nanomagnetics Characterization Facility. NMR spectra were obtained on Bruker EMX-200 FT-NMR spectrometers. Electron spin resonance spectra were obtained on a Bruker ESP-300 spectrometer equipped with computer interface for data acquisition and workup. All chemicals and solvents were used as obtained from the manufacturers unless otherwise stated.

1-(4-(*N*-*tert*-Butyl-*N*-[*tert*-butyldimethylsiloxyl]amino)phenyl)-1*H*-1,2,4-triazole (8). A round-bottom flask was charged with 0.97 g (3.0 mmol) of **7**,[13] 0.1 g (1.5 mmol) of 1,2,4-triazole, 0.24 mL (3.0 mmol) of pyridine, 0.41 g (2.25 mmol) of anhydrous copper acetate, and approximately 20 3 Å molecular sieves, and 20 mL of dichloromethane was added. The round-bottom flask was fitted with a drying tube containing Drierite and was allowed to stir for 3 days in air. The resulting mixture was filtered through Celite, and the plug was washed with dichloromethane and methanol. The combined organic layers were dried with $MgSO_4$, filtered and concentrated in vacuo onto silica gel, and chromatographed with a mixture of 30:70 ethyl acetate/hexane. Compound **8** was isolated as a yellow oil (0.14 g, 27%). ^1H NMR (200 MHz, $CDCl_3$) δ −0.10 (br s, 6 H); 0.92 (s, 9 H); 1.12 (s, 9 H); 7.55 (d, 2 H, $J = 8.5$ Hz); 7.38 (d, 2 H, $J = 7.9$ Hz); 8.10 (s, 1 H); 8.52 (s, 1 H).

1-(4-(*N*-*tert*-Butyl-*N*-hydroxylaminophenyl))-1*H*-1,2,4-triazole (9). To a solution of 0.126 g (0.364 mmol) of **70** in 5 mL of ethanol was added 1 mL of concentrated HCl. The resulting solution was stirred overnight under argon. The solution was concentrated in vacuo, then diluted with 5 mL of water, neutralized to pH 5 with 1 M aqueous NaOH, and then extracted repeatedly with dichloromethane. The organic layers were combined, washed with water and then brine, dried over magnesium sulfate, filtered, and concentrated in vacuo to give **9** as a white powder (0.83 g, 99%). The sample turned red upon heating and then melted at 141−143 °C. ^1H NMR (200 MHz, $CDCl_3$) δ 1.13 (s, 9 H); 6.54 (s, 1 H); 7.33 (d, 2 H, $J = 8.9$ Hz); 7.51 (d, 2 H, $J = 8.9$ Hz); 8.06 (s, 1 H), 8.47 (s, 1 H).

1-(4-(*N*-*tert*-Butyl-*N*-aminoxylphenyl))-1*H*-1,2,4-triazole (2). Lead dioxide (0.094 g, 0.39 mmol) was added to a solution of 0.076 g (0.33 mmol) of **9** in 5 mL of ethyl acetate. The resulting suspension was stirred for 1 h under argon. The suspension was then filtered through Celite and the filtrate concentrated in vacuo, and the resulting oil was recrystallized from a mixture of dichloromethane and hexane under air to give red needle crystals (0.030 g, 40%). Mp 69−71 °C. ESR (benzene): $g = 2.0056$, $a_N = 11.30$ (nitroxide N); $a_H = 2.34$ (2H), 0.93 (2H), 0.11 (1H); $a_N = 0.43$ (1N), 0.18 (1N) G. UV (THF): $\lambda = 315$ nm, $\epsilon = 66\,000$ M^{-1} cm^{-1}; $\lambda = 500$ nm, $\epsilon = 3200$ M^{-1} cm^{-1}. Crystallographic information is given in the Supporting Information, and the CCDC deposition number is 215554.

1:1 Cu/Triazole Radical Complex (3). A solution of 0.070 g (0.14 mmol) of $Cu(hfac)_2 \cdot 3H_2O$ in 4 mL of dichloromethane and 8 mL of hexane was layered on top of 0.034 g (0.14 mmol) of radical **72** in 4 mL of dichloromethane. The resulting layers were allowed to mix and evaporate slowly to yield 4 mg (4%) of small, dark green, cubelike crystals. Crystal data: $C_{22}H_{17}F_{12}CuN_4O_5$, $M = 708.917$, triclinic, $P\bar{1}$, $a = 10.1436(3)$ Å, $b = 10.3358(3)$ Å, $c = 14.9004(6)$ Å, $\alpha = 91.7513(11)°$, $\beta = 93.5277(13)°$, $\gamma = 114.6025(10)°$, $V = 1414.96(8)$ Å^3, $Z = 2$, $\mu = 0.891$ mm^{-1}, $T = 293$ K, data/parameters $= 4935/399$, converging to R1 $= 0.0694$, wR2 $= 0.1798$ (on 3305, $I > 2\sigma(I)$ observed data); R1 $= 0.1068$, wR2 $= 0.2060$ (all data), residual electron density 0.773 e/Å^3. The CCDC deposition number is 215556.

1:1 Mn/Triazole Radical Complex (4). A solution of 0.066 g (0.14 mmol) of $Mn(hfac)_2 \cdot 3H_2O$ in 4 mL of dichloromethane and 8 mL of hexane was layered on top of 0.034 g (0.14 mmol) of radical **72** in 4 mL of dichloromethane. The resulting layers were allowed to mix and evaporate slowly to yield 0.042 g (42%) of dark red platelike crystals, mp 183−185 °C. Anal. Calcd for $C_{22}H_{17}N_4O_5F_{12}Mn$: C, 37.73; H, 2.45; N, 8.00. Found: C, 37.23; H, 2.32; N, 7.72. Crystal data: $C_{22}H_{17}F_{12}Mn_1N_4O_5$, $M = 700.315$, triclinic, $P\bar{1}$, $a = 9.7111(2)$ Å, $b = 10.6775(3)$ Å, $c = 14.7440(6)$ Å, $\alpha = 93.1757(12)°$, $\beta = 91.2499(12)°$, $\gamma = 114.458(2)°$, $V = 1387.80(7)$ Å^3, $Z = 2$, $\mu = 0.597$ mm^{-1}, $T = 293$ K, data/parameters $= 4874/397$, converging to R1 $= 0.0692$, wR2 $= 0.1900$ (on 3700, $I > 2\sigma(I)$ observed data); R1 $= 0.0927$, wR2 $= 0.2027$ (all data), residual electron density 0.993 e/Å^3. The CCDC deposition number is 215553.

11:1 Ni/Triazole Radical Complex (5). A solution of 0.051 g (0.108 mmol) of $Ni(hfac)_2 \cdot xH_2O$ in 4 mL of dichloromethane and 8 mL of hexane was layered on top of 0.026 g (0.108 mmol) of radical **72** in 4 mL of dichloromethane. The resulting layers were allowed to mix and evaporate slowly to yield 0.030 g (40%) dark needle-shaped crystals. Upon heating, the sample decomposed slowly and then melted at 208−212 °C. Anal. Calcd for $C_{22}H_{17}N_4O_5F_{12}Ni$: C, 37.53; H, 2.43; N, 7.96. Found: C, 37.50; H, 2.16; N, 7.90. Crystal data: $C_{22}H_{17}F_{12}NiN_4O_5$, $M = 704.087$, triclinic, $P\bar{1}$, $a = 9.8155(2)$ Å, $b = 10.5185(2)$ Å, $c = 15.0198(3)$ Å, $\alpha = 93.1995(7)°$, $\beta = 92.5002(8)°$, $\gamma = 116.6025(8)°$, $V = 1380.29(5)$ Å^3, $Z = 2$, $\mu = 0.825$ mm^{-1}, $T = 293$ K, data/parameters $= 4819/399$, converging to R1 $= 0.0492$, wR2 $= 0.1315$ (on 4320, $I > 2\sigma(I)$ observed data); R1 $= 0.0545$, wR2 $= 0.1375$ (all data), residual electron density 0.254 e/Å^3. The CCDC deposition number is 215557.

11:1 Co/Triazole Radical Complex (6). A solution of 0.051 g (0.108 mmol) of $Co(hfac)_2 \cdot xH_2O$ in 4 mL of dichloromethane and 8 mL of hexane was layered on top of 0.026 g (0.108 mmol) of radical **72** in 4 mL of dichloromethane. The resulting layers were allowed to mix and evaporate slowly to yield 0.033 g (43%) of dark green, needle-shaped crystals, mp 171−173 °C. Anal. Calcd for $C_{22}H_{17}N_4O_5F_{12}Co$: C, 37.52; H, 2.43; N, 7.96. Found: C, 37.42; H, 2.39; N, 7.87. Crystal data: $C_{22}H_{17}F_{12}CoN_4O_5$, $M = 704.310$, triclinic, $P\bar{1}$, $a = 9.73670(10)$ Å, $b = 10.5646(2)$ Å, $c = 14.8865(3)$ Å, $\alpha = 93.0482(6)°$, $\beta = 91.6094(6)°$, $\gamma = 115.4709(10)°$, $V = 1378.29(10)$ Å^3, $Z = 2$, $\mu = 0.745$ mm^{-1}, $T = 293$ K, data/parameters $= 4833/397$, converging to R1 $= 0.0526$, wR2 $= 0.1414$ (on 4289, $I > 2\sigma(I)$ observed data); R1 $= 0.0588$, wR2 $= 0.1484$ (all data), residual electron density 0.862 e/Å^3. The CCDC deposition number is 215555.

(13) Compound **7** was made as described in: Liao, Y.; Xie, C.; Lahti, P. M.; Weber, R. T.; Jiang, J.; Barr, D. P. *J. Org. Chem.* **1999**, *64*, 5176.

Supporting Information Available: ESR summary for **2** and spin density computations for radicals **1**, **2**, and **12**, as well as crystallographic information in CIF format for **2**−**6**. This material is available free of charge via the Internet at http://pubs.acs.org.

IC0349050